Supplementary information

Chlamydia-like bacterium *Simkania negevensis* exploits host sphingolipid salvage pathway and sphingomyelin synthesis during infection

Arpita Mohanty[1,†], Jonas D. Weinrich[1,†], Fabian Schumacher[2], Marcel Rühling[1,‡], Sanisha Sunuwar[1], Helena Szegedi[1], Dominik Wigger[2,§], Fabio Schmelz[1], Bapin Kumar Panda[3], Christian Kappe[4], Daniela Brenner[5], Melanie Schirmer[6,7,8], Christoph Arenz[4], Jürgen Seibel[5], Joost C. M. Holthuis[3], Sudip Das[6,7,8], Martin Fraunholz[1], Burkhard Kleuser[2], and Vera Kozjak-Pavlovic[1,*]

[1]*Department of Microbiology, Biocenter, Julius-Maximilians-Universität Würzburg, Würzburg, Germany.*
[2]*Institute of Pharmacy, Freie Universität Berlin, Berlin, Germany.*
[3]*Molecular Cell Biology Division, Department of Biology and Center of Cellular Nanoanalytics, Osnabrück University, Osnabrück, Germany*
[4]*Institute of Chemistry, Humboldt-Universität zu Berlin, Berlin, Germany.*
[5]*Institute of Organic Chemistry, Julius-Maximilians-University Würzburg, Würzburg, Germany.*
[6]*Translational Microbiome Data Integration, School of Life Sciences, Technical University of Munich, Freising, Germany*
[7]*Center for Organoid Systems, Technical University Munich, Garching, Germany.*
[8]*ZIEL—Institute for Food & Health, Technical University of Munich, Freising, Germany.*

[†]These authors contributed equally

[‡] Present address: MRC Laboratory of Molecular Biology, Francis Crick Avenue, Cambridge Biomedical Campus, Cambridge CB2 0QH, UK

[§] Present address: Department of Veterinary Medicines, Federal Office of Consumer Protection and Food Safety, Berlin, Germany.

[*]Corresponding author: Vera Kozjak-Pavlovic; Biocenter, Am Hubland, D-97074 Würzburg, Germany; vera.kozjak@uni-wuerzburg.de

Table of Contents

Supplementary Methods

1. Processing and Statistical Analysis of Targeted Sphingolipidomics Data

a. Targeted lipidomics dataset

Lipid abundances were reported as absolute molar amounts per sample, expressed as pmol/sample. Biological replicates were analysed for each experimental condition.

The targeted panel was interpreted as a defined analytical panel rather than as a complete representation of total cellular lipid or total cellular sphingolipid content. Therefore, all downstream analyses were designed to preserve the quantitative meaning of the measured absolute abundances and to avoid post hoc transformations that would convert the data into compositional fractions of the measured panel [1, 2].

b. Use of absolute pmol/sample values for statistical comparison

Absolute pmol/sample values were retained as the main quantitative input for statistical testing. This approach was chosen because the experimental design already controlled the relevant denominator at the sample level. Specifically, samples were prepared from comparable biological input material, processed using the same extraction protocol, and analysed using the same targeted LC–MS/MS workflow. Internal standards added during extraction further supported control of extraction and ionisation-related technical variation [1].

When these conditions are satisfied, the measured pmol/sample value is directly interpretable as the amount of a given lipid species recovered from an equivalent sample. This makes the value suitable for comparing lipid abundance between experimental groups, provided that the biological input and sample-processing conditions are held constant.

No additional normalisation to the sum of measured lipids was applied before statistical testing. This was an intentional analytical decision, not an omission. Normalising each lipid to the total signal across the measured panel would change the biological meaning of the data from absolute abundance to within-panel composition. Such a transformation is not appropriate when the objective is to determine whether a lipid species or lipid class increases or decreases in absolute amount between conditions [1].

c. Rationale for not using alternative normalisation methods

An alternative approach sometimes used in targeted lipidomics is to sum all measured lipid species within each sample and express each lipid as a fraction of this measured total:

lipid pmol/sample ÷ sum of measured lipid pmol/sample

This transformation was not used for inferential testing because the denominator has limited biological interpretability. The measured panel contains lipid species from multiple sphingolipid classes with distinct biochemical roles, subcellular localisations, turnover rates, and abundance ranges. Therefore, the summed value represents an LC–MS/MS panel-defined total, not total lipid, total sphingolipid, total membrane content, or any coherent biological pool.

The panel is also incomplete by design. It captures selected detectable lipid species rather than the full cellular lipidome. Consequently, the denominator reflects only the measured

species and should not be interpreted as total cellular sphingolipid, total ceramide, total sphingomyelin, or total lipid content.

In addition, this normalisation introduces compositional closure: all lipid values become mathematically dependent because they share the same within-sample denominator. A change in a high-abundance lipid class can make lower-abundance lipids appear relatively depleted even when their absolute pmol/sample values are unchanged, and vice versa [3].

Finally, cross-class row-sum normalisation can distort biologically relevant changes in low-abundance signalling lipids or pathway intermediates. If the denominator is dominated by abundant structural lipids, changes in lower-abundance species may be compressed or misrepresented. For these reasons, absolute pmol/sample values were retained for inferential analysis [1, 3].

d. Log_{10} transformation before statistical testing

Before inferential testing, absolute pmol/sample values were transformed using:

$\log_{10}(x + 1)$,

where x is the measured pmol/sample value for a given lipid in a given sample.

This transformation combines two distinct operations. The $\log_{10}$ component changes the statistical scale of the positive abundance values, while the +1 offset allows zero-valued observations to remain mathematically defined. Importantly, this transformation does not normalise the data to total lipid, total sphingolipid, or any within-sample lipid sum. The biological denominator remains the original sample [1, 3].

The $\log_{10}$ transformation was used because lipidomics abundance data are commonly right-skewed. A small number of high-abundance measurements can dominate group means, variances, and statistical tests on the raw scale. Log transformation compresses the upper range of the distribution and reduces scale-dependent variation, making the data more suitable for statistical comparison, particularly when sample sizes are modest [1, 3].

The +1 offset was included to handle zero-valued measurements. Since $\log_{10}(0)$ is undefined, zero values would otherwise become infinite or unusable in downstream statistics [2, 4, 5].

Thus, the purpose of $\log_{10}(x + 1)$ was to improve statistical behaviour while retaining the original absolute-abundance framework. It should not be interpreted as a compositional or total-lipid normalisation step [2, 4, 5].

e. Statistical comparison between experimental conditions

Statistical testing was performed on the $\log_{10}(x + 1)$-transformed pmol/sample values. For each lipid species or lipid-class summary, comparisons were made between predefined experimental groups according to the experimental design. Where multiple pairwise comparisons were performed, p-values were adjusted for multiple testing using a false discovery rate (FDR) procedure [1].

Effect estimates from pairwise comparisons were used to summarise the direction and magnitude of differences between groups. A positive estimate indicates that the first group in

the contrast has a higher transformed abundance than the second group. A negative estimate indicates that the first group has a lower transformed abundance than the second group.

Non-significant pairwise comparisons after FDR correction were not interpreted as confirmed biological changes, even if a numerical estimate was present. In visual summaries, these comparisons may be masked in grey or labelled as non-significant.

Supplementary Figures

Supplementary Figure 1

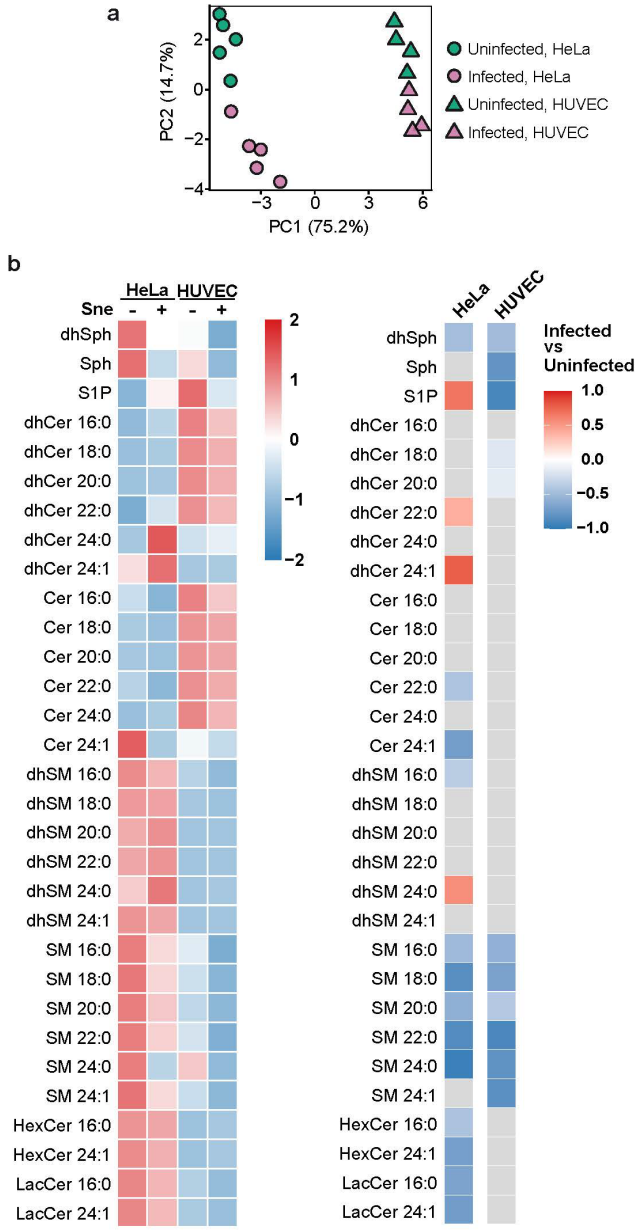

Supp. Fig. 1. Species-level sphingolipid remodeling in HeLa and HUVEC cells during Sne infection. HeLa and HUVEC cells were infected with Sne for 3 or 2 days, respectively, at MOI 1. Lipids were extracted with methanol and analyzed by LC-MS/MS. Lipid abundances were quantified as pmol/sample. For statistical testing, values were transformed as $\log_{10}(x + 1)$. **(a)** Principal component analysis (PCA) of individual sphingolipid species abundances $\log_{10}(x + 1)$-transformed pmol/sample in uninfected (green) and infected (purple) HeLa (n = 5) and HUVEC cells (n = 4). PCA was performed on mean-centered and unit-variance-scaled data. Samples segregate primarily by cell type along PC1 (75.2 %) and by infection status along PC2 (14.7 %), Symbols denote cell type (circles, HeLa; triangles, HUVEC) and colors denote infection status (green, uninfected; magenta, infected). **(b)** Heatmaps show row-wise z-scores calculated on $\log_{10}(x + 1)$-transformed pmol/sample values (left panel) in uninfected (Sne -) and infected (Sne +) HeLa (n = 5) and HUVEC cells (n = 4). Heatmap showing pairwise group comparisons performed on $\log_{10}(x + 1)$-transformed pmol/sample values between the indicated experimental conditions (right panel), represented as $\log_2$ values (infected - uninfected) with *p*-value adjusted for False-Discovery Rate (FDR). Values are displayed ranging from blue (decrease) to red (increase), with white indicating no change. Non-significant comparisons (FDR ≥ 0.05) are masked (grey).

Supplementary Figure 2

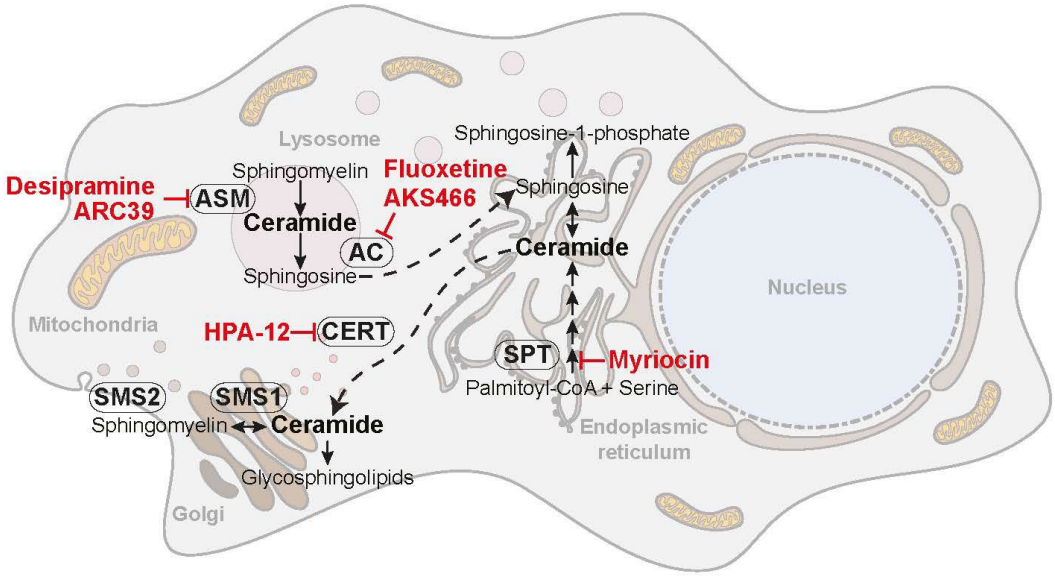

154

155 **Supp. Fig. 2. Overview of sphingolipid metabolic pathways and experimental perturbations.** Schematic overview
156 of host sphingolipid metabolic pathways targeted in this study and corresponding pharmacological and genetic
157 perturbations used to investigate *S. negevensis* infection. Myriocin blocks *de novo* ceramide synthesis through serine
158 palmitoyltransferase (SPT) inhibition. ARC39 and desipramine inhibit acid sphingomyelinase (ASM)-dependent
159 sphingomyelin hydrolysis, whereas AKS466 and fluoxetine target acid ceramidase (AC)-associated ceramide
160 catabolism. HPA-12 inhibits CERT-mediated non-vesicular ceramide trafficking from the endoplasmic reticulum to the
161 Golgi apparatus. The contribution of sphingomyelin synthase activity was assessed using SMS1/2 double knockout
162 (dko) cells carrying inducible complementation constructs or catalytically impaired SMS2 mutants.

163

Supplementary Figure 3

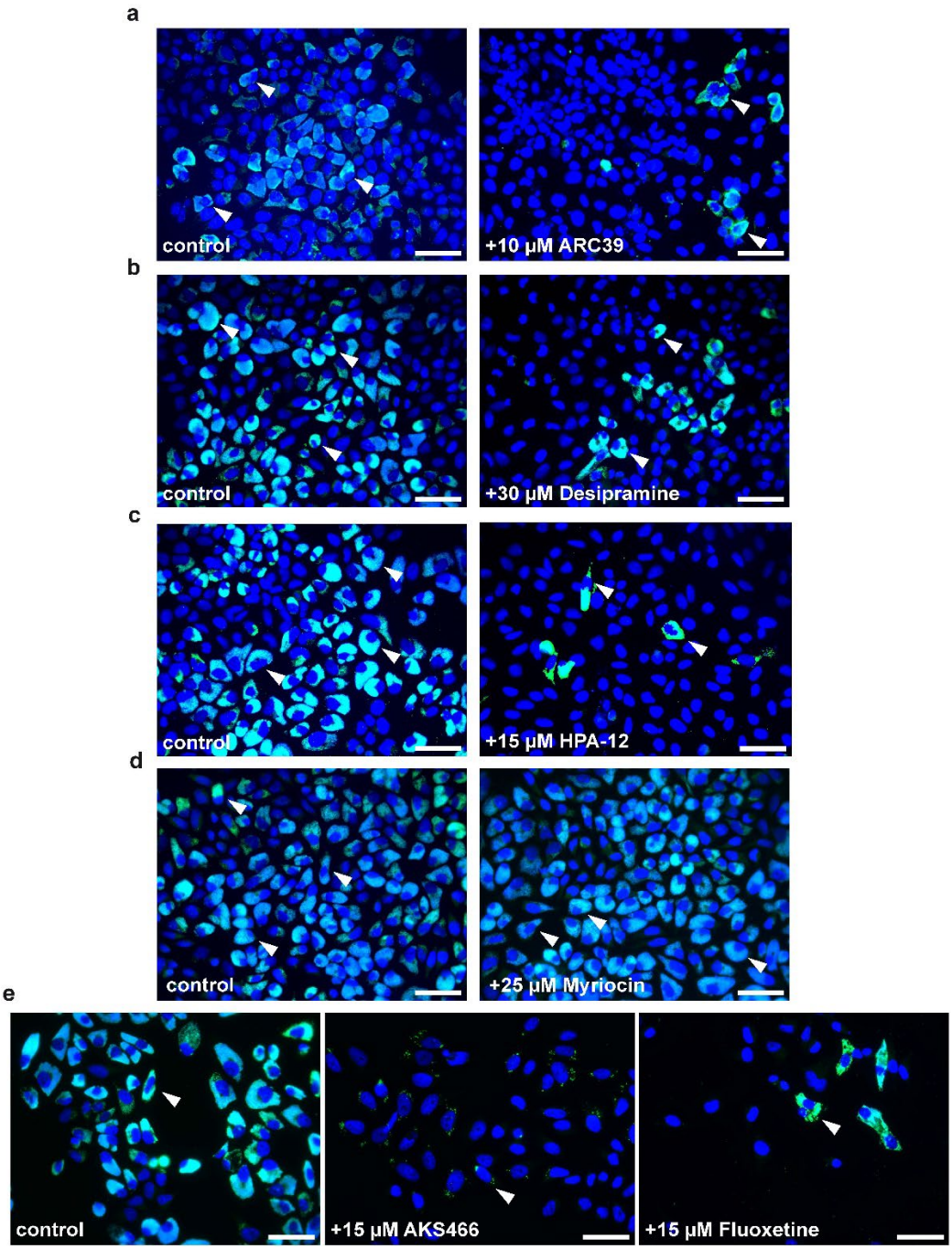

Supp. Fig. 3. **Inhibition of sphingolipid pathways alters Sne infection and vacuole morphology.** Representative fluorescence microscopy images of HeLa cells following inhibition of sphingolipid metabolism pathways. Cells were pre-treated with the indicated inhibitors for 3 h and were infected with Sne (MOI = 1) for 72 h in the presence of inhibitors. Cells were fixed and stained with DAPI (blue) and an anti-*S. negevensis* (Sn) GroEL (green). Representative infected cells were indicated by white arrowheads. Solvent-treated cells were used as controls. Scale bar, 50 µm. **(a)** Direct inhibition of ASM using ARC39 (10 µM). **(b)** Indirect ASM inhibition using desipramine (30 µM). **(c)** Inhibition of ceramide transport via CERT using HPA-12 (15 µM). **(d)** Inhibition of *de novo* ceramide synthesis using myriocin (25 µM) **(e)** Inhibition of acid ceramidase (AC) using AKS466 (15 µM) or fluoxetine (15 µM).

Supplementary Figure 4

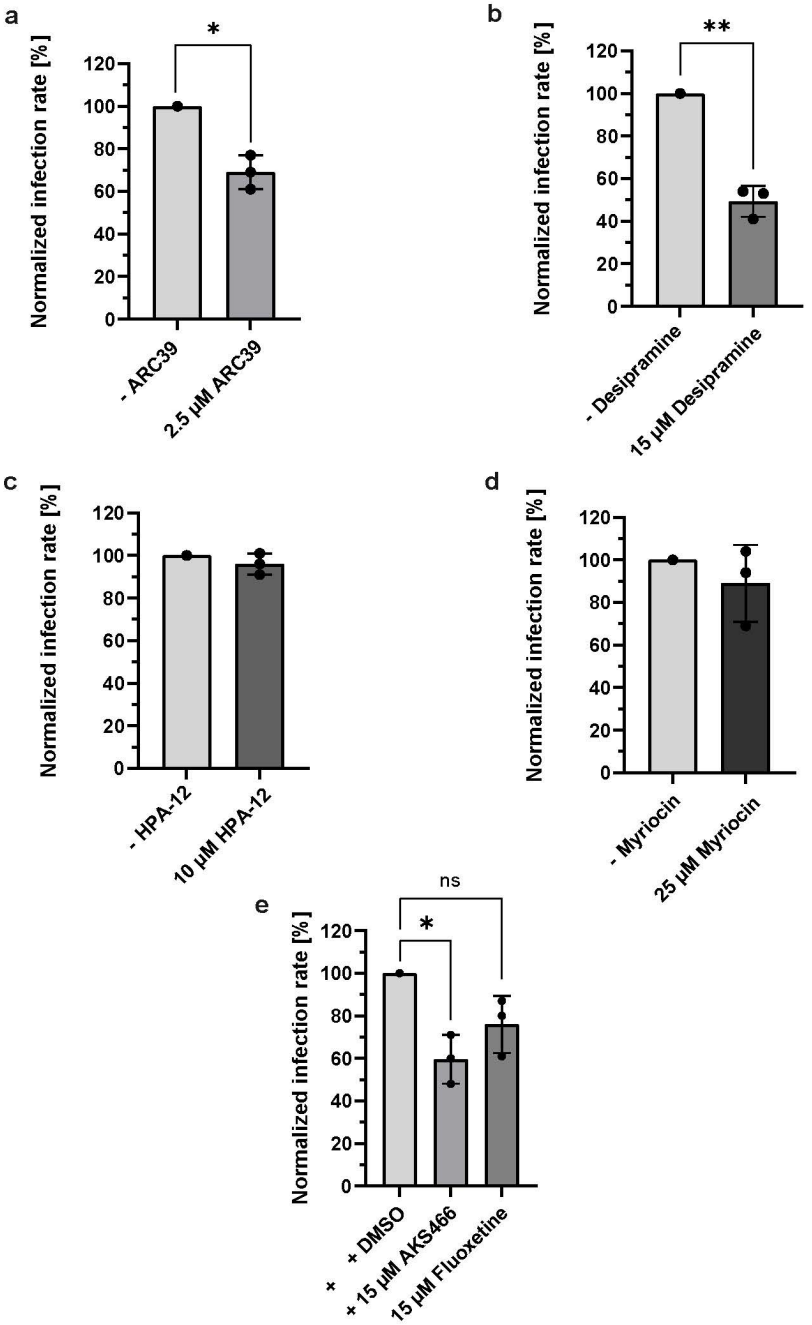

Supp. Fig. 4. Late-stage inhibition of sphingolipid metabolism has a limited effect on Sne infection. Infection rates in HeLa cells when infected with Sne *(*MOI = 1) following treatment with the indicated inhibitors 6 h p.i. **(a)** Direct inhibition of ASM using ARC39 (2.5 µM). **(b)** Indirect ASM inhibition using desipramine (15 µM). **(c)** Inhibition of ceramide transport via CERT using HPA-12 (10 µM). **(d)** Inhibition of *de novo* ceramide synthesis using myriocin (25 µM). **(e)** Inhibition of acid ceramidase (AC) using AKS466 (15 µM) or fluoxetine (15 µM). Infection rates were averaged per well, normalized to the respective solvent control. Bars depict mean ± SD. n = 3. Statistical analysis was performed using one-sample t-test and Wilcoxon test (*p ≤ 0.05, **p ≤ 0.01, ***p ≤ 0.001).

Supplementary Figure 5

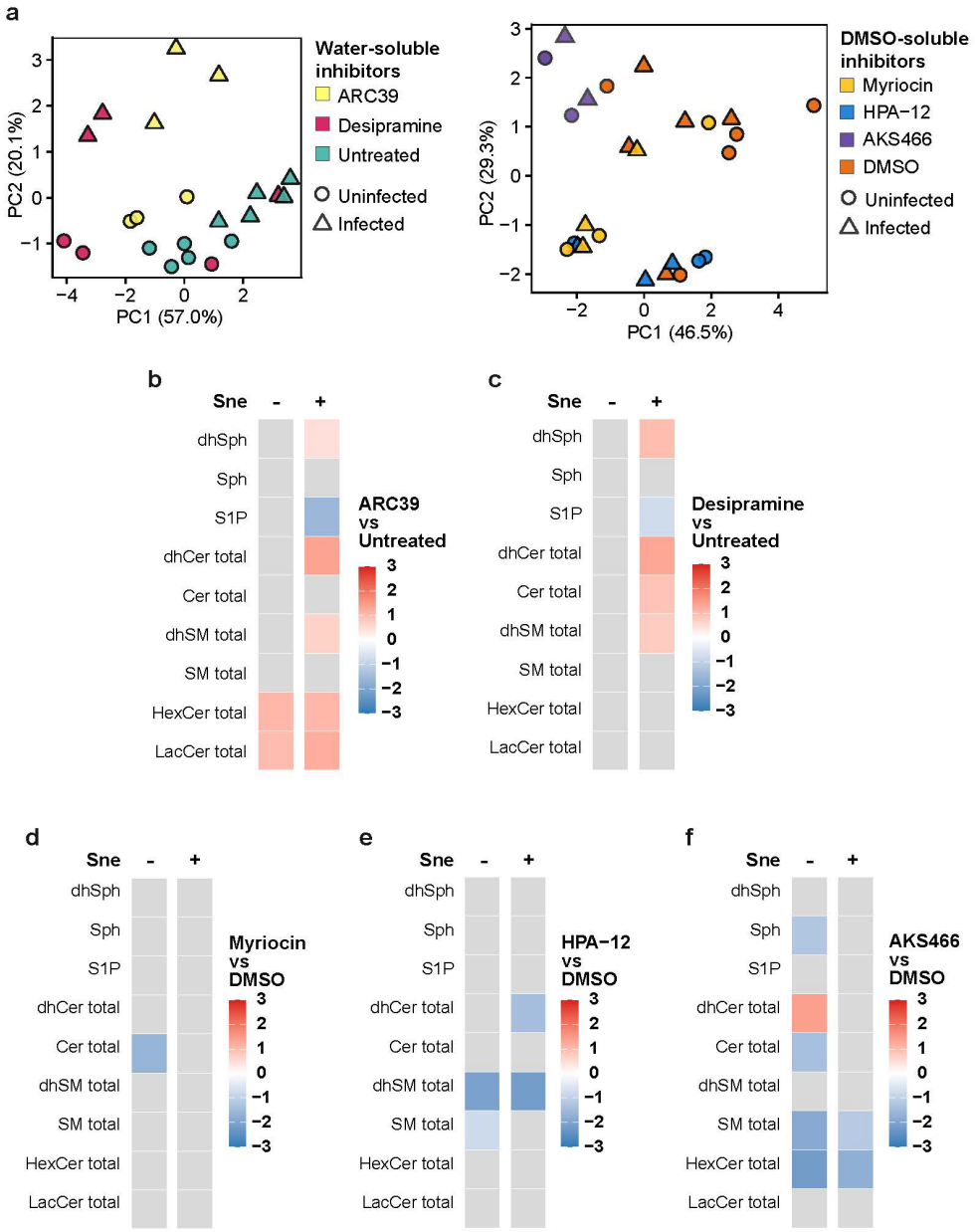

Supp. Fig. 5. Sphingolipid remodeling during pharmacological pathway inhibition. HeLa cells treated with sphingolipid pathway inhibitors were either left uninfected or infected with Sne (MOI = 1). Lipids were extracted with methanol and analyzed by LC-MS/MS. Lipid abundances were quantified as pmol/sample. For statistical testing, values were transformed as $\log_{10}(x + 1)$. **(a)** PCA of sphingolipid abundances from uninfected HeLa cells, $\log_{10}(x + 1)$-transformed pmol/sample, was performed on mean-centered and unit-variance-scaled data. The left panel shows lipidome from cells treated with water-soluble ASM inhibitors: ARC39 (yellow) and desipramine (red) or left untreated (teal). The separation along PC1 (57.0 %) and PC2 (20.1 %) reflects inhibitor-associated variance. The right panel shows the sphingolipid profile of cells treated with DMSO-soluble inhibitors: AKS466 (purple), HPA-12 (blue), myriocin (yellow), and control (orange, DMSO). The separation along PC1 (46.5 %) and PC2 (29.3 %) reflects inhibitor-dependent remodeling of the sphingolipid profile. Circles represent individual biological replicates, and colors indicate treatment. **(b–f)** Heatmaps showing pairwise group comparisons performed on $\log_{10}(x + 1)$-transformed pmol/sample values between uninfected and infected conditions, following pharmacological inhibition. Values were represented as $\log_2$ relative to untreated or vehicle controls (ARC39 vs untreated; desipramine vs untreated; HPA-12 vs DMSO; myriocin vs DMSO; AKS466 vs DMSO), with p values adjusted for FDR. Rows represented sphingolipid classes and columns represented infection status. Red and blue indicate relative increase or decrease in sphingolipid species; non-significant comparisons (FDR ≥ 0.05) masked (grey).

Supplementary Figure 6

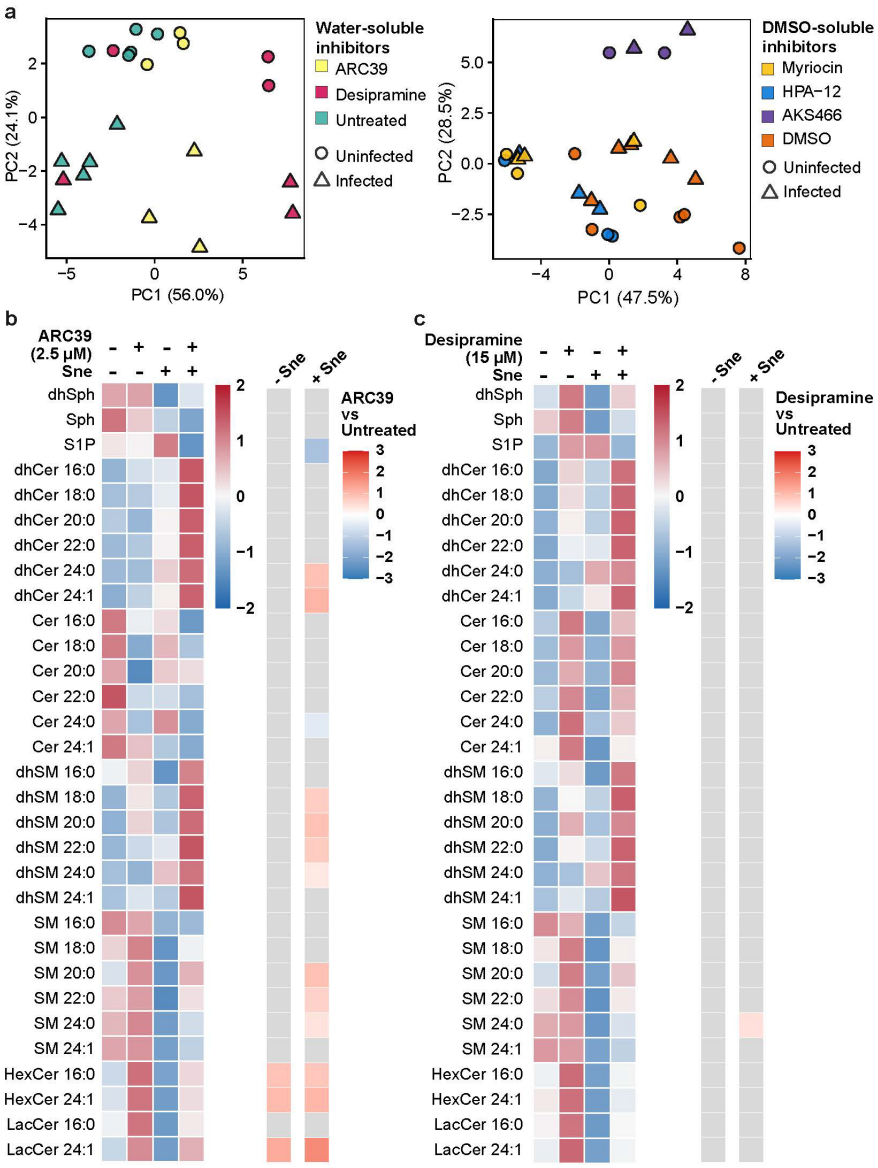

Supp. Fig. 6. Species-level sphingolipid remodeling under ASM inhibition. Lipids were extracted with methanol and analyzed by LC-MS/MS. Lipid abundances were quantified as pmol/sample. For statistical testing, values were transformed as $\log_{10}(x + 1)$. Principal component analysis (PCA) of individual sphingolipid species abundances $\log_{10}(x + 1)$-transformed pmol/sample from uninfected (circles) and infected (triangles) HeLa cells was performed on mean-centered and unit-variance-scaled data. **(a)** Lipidome from cells treated with water-soluble ASM inhibitors; (left panel) ARC39 (yellow) and desipramine (red) or left untreated (teal) shows separation primarily along PC1 (56.0 %) and PC2 (24.1 %), reflecting inhibitor-associated variance. along PC1 (47.5 %) and PC2 (28.5 %), indicating inhibitor-dependent remodeling of the sphingolipid profile. Sphingolipid profile of cells treated with DMSO-soluble inhibitors; (right panel) AKS466 (purple), HPA-12 (blue), myriocin (yellow), and control (orange, DMSO), shows separation along PC1 (47.5 %) and PC2 (28.5 %), indicating inhibitor-dependent remodeling of the sphingolipid profile. Circles represent individual biological replicates, and colors indicate treatment. **(b, c)** Heatmap showing row-wise z-scores calculated on $\log_{10}(x + 1)$-transformed pmol/sample values of individual shingolipid species, following ARC39 (b) or desipramine (c) inhibition under uninfected (Sne -) and infected (Sne +) conditions (left panel). Heatmap of pairwise group comparisons performed on $\log_{10}(x + 1)$-transformed pmol/sample values (right panel) represented as $\log_2$ (infected vs uninfected) with p-value adjusted for False-Discovery Rate (FDR). Values are displayed ranging from blue (decrease) to red (increase), with white indicating no change and non-significant comparisons (FDR ≥ 0.05) masked (grey).

Supplementary Figure 7

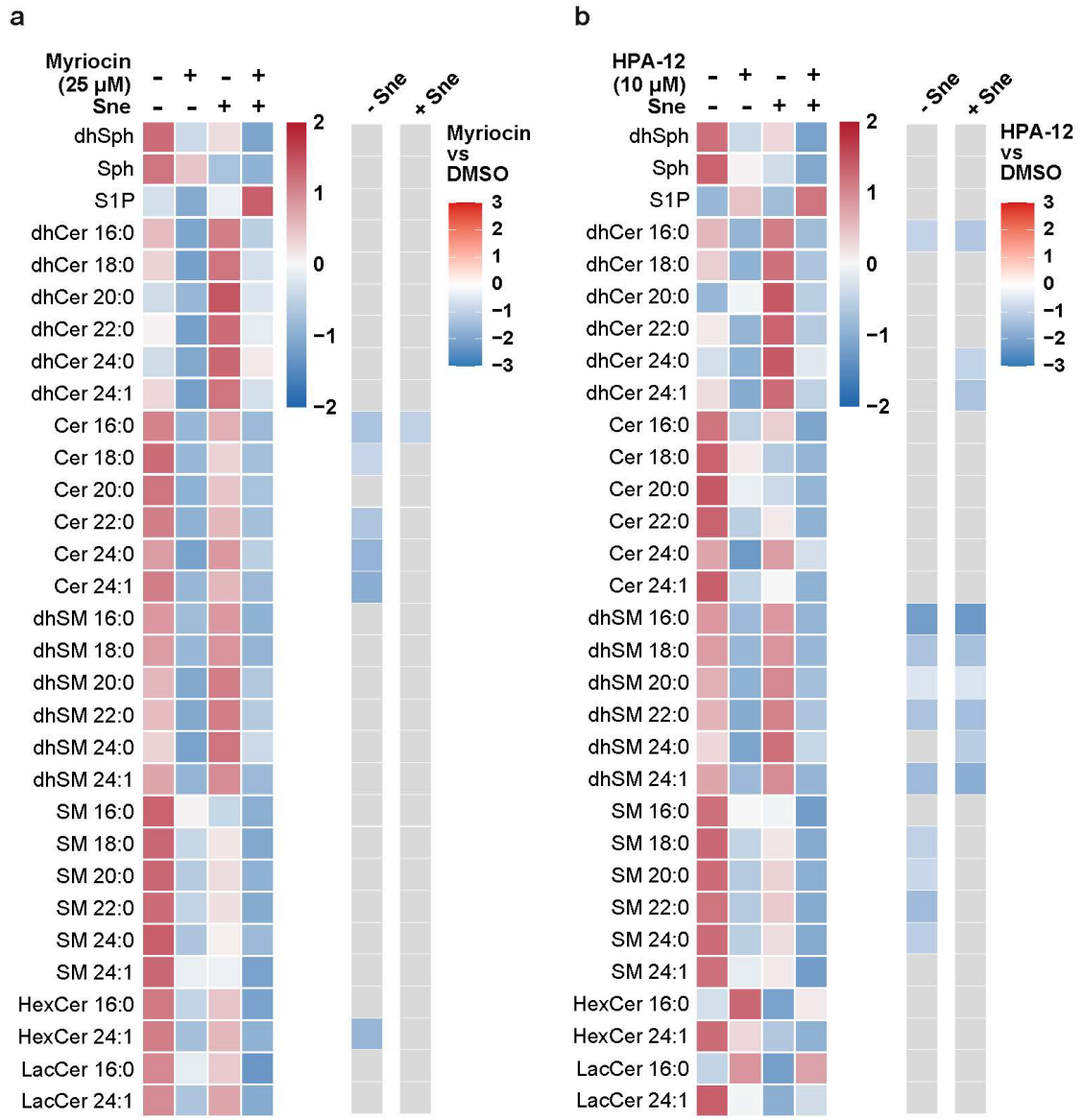

Supp. Fig. 7. Species-level sphingolipid remodeling under myriocin and HPA-12 treatment. Lipids were extracted with methanol and analyzed by LC-MS/MS. Lipid abundances were quantified as pmol/sample. For statistical testing, values were transformed as $\log_{10}(x + 1)$. **(a, b)** Heatmap showing row-wise z-scores calculated on $\log_{10}(x + 1)$-transformed pmol/sample values of individual shingolipid species following myriocin (a) or HPA-12 (b) inhibition under uninfected (Sne -) and infected (Sne +) conditions (left panel). Right panels depict heatmaps of pairwise group comparisons performed on $\log_{10}(x + 1)$-transformed pmol/sample values represented as $\log_2$ (infected vs. uninfected) with p-value adjusted for False-Discovery Rate (FDR). Values are displayed ranging from blue (decrease) to red (increase), with white indicating no change, and non-significant comparisons (FDR ≥ 0.05) masked (grey).

Supplementary Figure 8

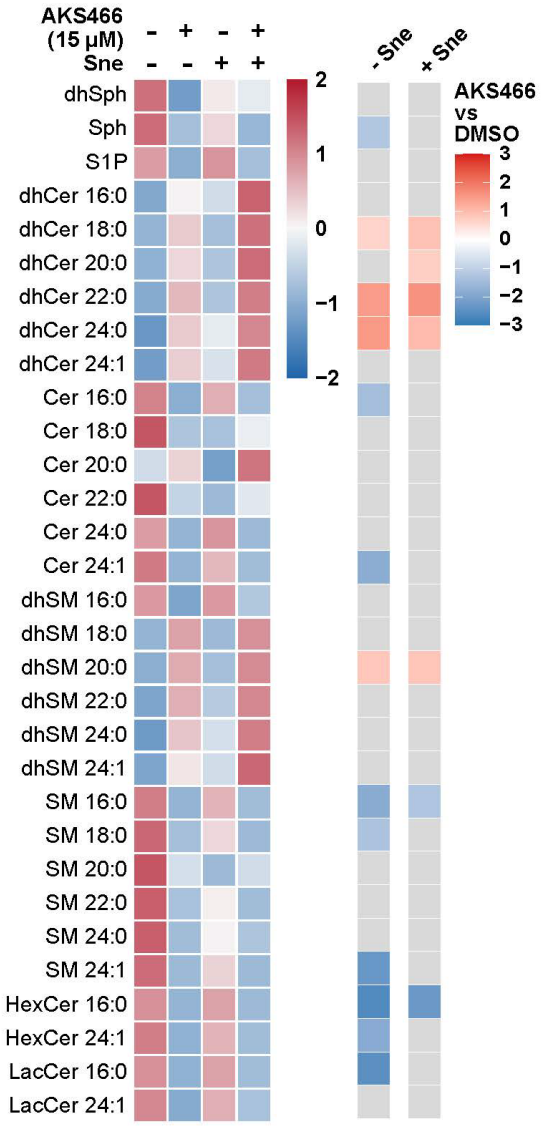

224

225 **Supp. Fig. 8. Species-level sphingolipid remodeling under AKS466 treatment.** Lipids were extracted with
226 methanol and analyzed by LC-MS/MS. Lipid abundances were quantified as pmol/sample. For statistical testing, values
227 were transformed as $\log_{10}(x + 1)$. Heatmap showing row-wise z-scores calculated on $\log_{10}(x + 1)$-transformed
228 pmol/sample values of individual shingolipid species following AKS466 inhibition under uninfected (Sne -) and infected
229 (Sne +) conditions (left panel). Heatmap of pairwise group comparisons performed on $\log_{10}(x + 1)$-transformed
230 pmol/sample values (right panel) represented as $\log_2$ (infected vs. uninfected) with p-value adjusted for False-
231 Discovery Rate (FDR). Values are displayed ranging from blue (decrease) to red (increase), with white indicating no
232 change, and non-significant comparisons (FDR ≥ 0.05) masked (grey).

Supplementary Figure 9

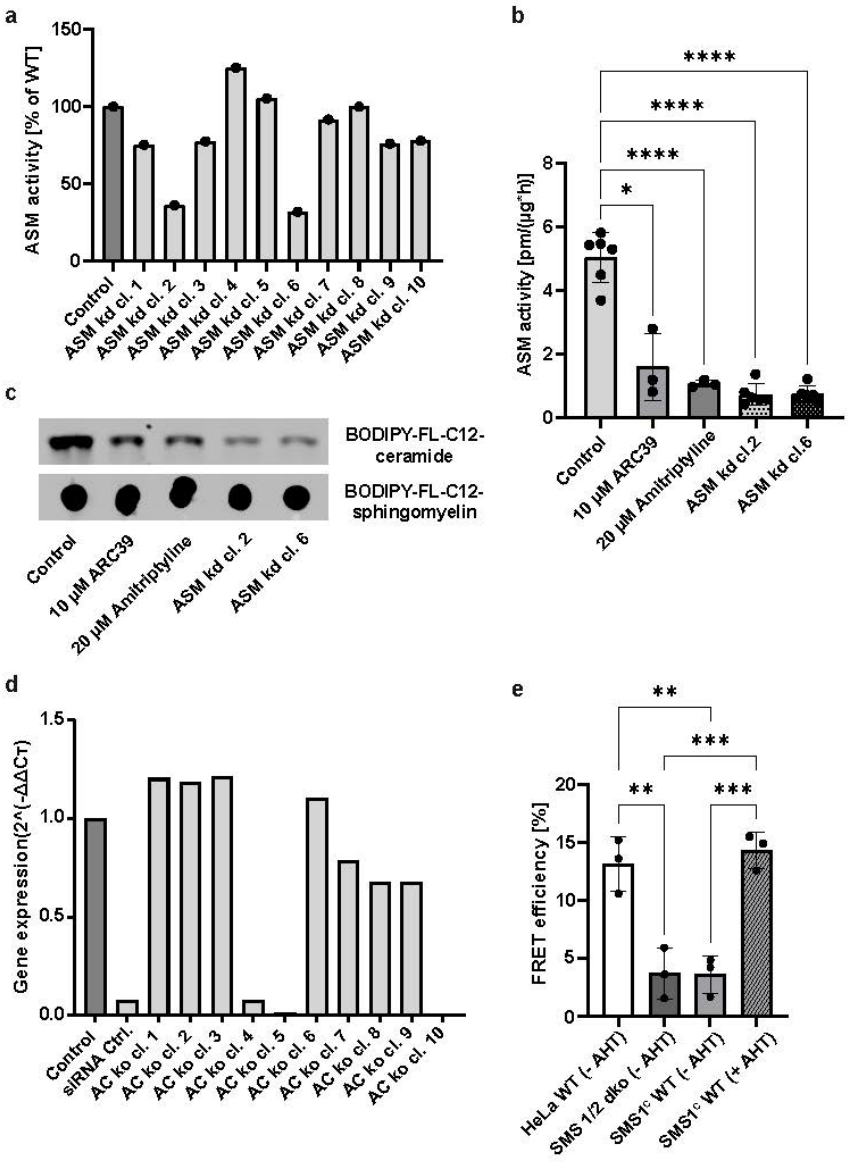

Supp. Fig. 9. Validation of genetically modified sphingolipid metabolism cell lines. (a) Screening of clones with the shRNA-mediated knockdown of acid sphingomyelinase (ASM kd). ASM activity was measured and normalized to the HeLa WT control. **(b)** ASM activity was quantified in inhibitor-treated (ARC39 10 µM; amitriptyline, 20 µM) cells and ASM kd clones compared with control cells. The graphs show mean value ± SD, (n = 3). Statistical significance was determined using one-way ANOVA followed by multiple comparisons. *p ≤ 0.05; ****p ≤ 0.0001. **(c)** Representative thin-layer chromatography (TLC) analysis using BODIPY-FL-C12–labelled ceramide. Reduced conversion to sphingomyelin was observed upon ASM inhibition (ARC39, 10 µM; amitriptyline, 20 µM) and in ASM kd clones (cl.2 and cl.6), confirming the knockdown. **(d)** Validation of AC ko clones by gene expression analysis. Relative expression levels (2^(−ΔΔCT)) confirmed efficient depletion of AC expression in selected knockout clones compared with control and *ASAH1*-siRNA-kd control. **(e)** Validation of sphingomyelin synthase 1 (SMS1) activity using a FRET-based assay. HeLa WT, SMS1/2 dko, and SMS1 WT complemented cells ($SMS1^{C}$ WT) were analysed in the absence or presence of AHT induction. FRET efficiency was determined by FRET acceptor bleaching. Bar graphs show mean ± SD, (n = 3). Statistical significance was assessed using One-way ANOVA followed by Šídák's multiple comparison. *p < 0.05; **p < 0.01; ***p < 0.001; ns, not significant.

Supplementary Figure 10

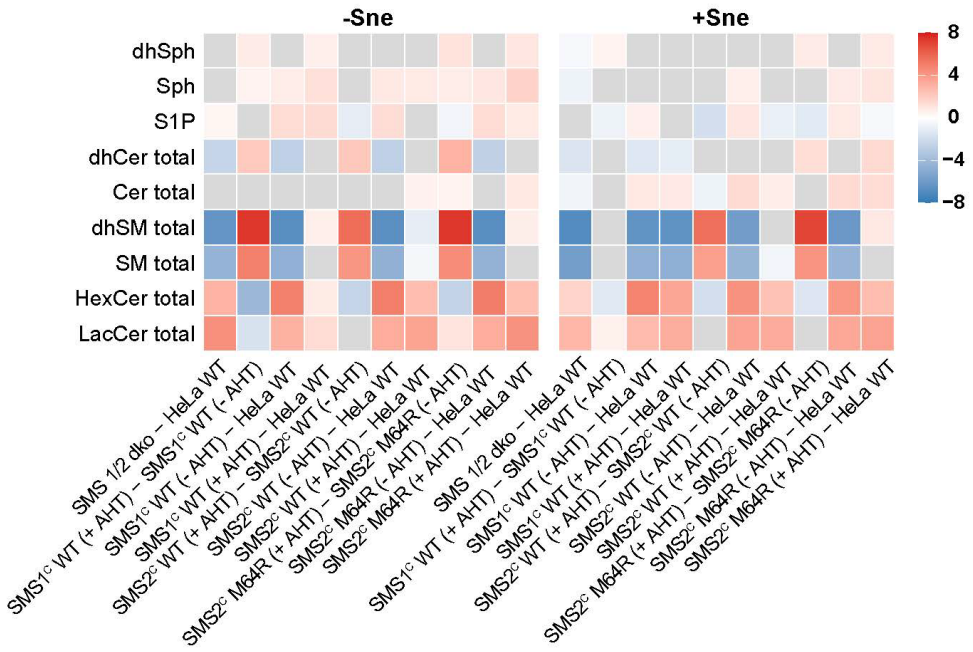

Supp. Fig. 10. Differential sphingolipid class remodeling across SMS genotypes. Lipids were extracted with methanol and analyzed by LC-MS/MS. Lipid abundances were quantified as pmol/sample. For statistical testing, values were transformed as $\log_{10}(x + 1)$. Heatmap showing pairwise group comparisons performed on $\log_{10}(x + 1)$-transformed pmol/sample values across SMS-modified cell lines represented as $\log_2$ (uninfected, -Sne and infected +Sne) with p-value adjusted for FDR. Pairwise comparisons were performed between SMS1/2 dko, $SMS1^C$ WT, $SMS2^C$ WT, and $SMS2^C$ M64R cells relative to HeLa WT controls and under both AHT-induced (+AHT) and non-induced (-AHT) conditions. Values are displayed ranging from blue (decrease) to red (increase), with white indicating no change, and non-significant comparisons (FDR ≥ 0.05) masked (grey).

Supplementary Figure 11

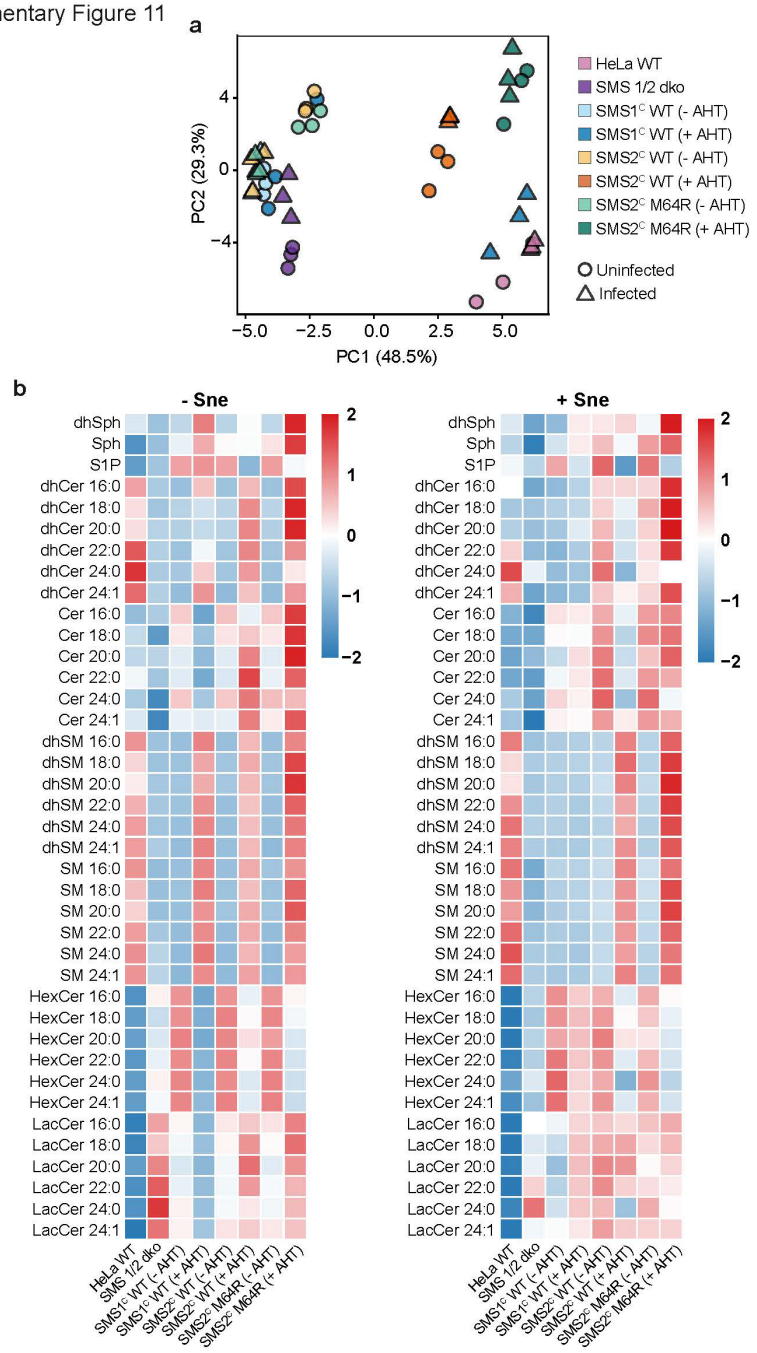

Supp. Fig. 11. SMS genotype-dependent remodeling of individual sphingolipid species. Lipids were extracted with methanol and analyzed by LC-MS/MS. Lipid abundances were quantified as pmol/sample. For statistical testing, values were transformed as $\log_{10}(x + 1)$. **(a)** PCA analysis of individual sphingolipid abundances was performed on $\log_{10}(x + 1)$-transformed pmol/sample values across SMS1/2 genotypes (HeLa WT, SMS1/2 dko, SMS1^{C} WT (-/+AHT), SMS2^{C} WT (-/+AHT), and SMS2^{C} M64R (-/+AHT), in uninfected (circle) and infected (triangle) conditions (n = 3). Samples segregated along PC1 (48.5 %) and PC2 (29.3 %), reflecting differences associated with SMS genotype, AHT-dependent induction, and infection status. Colors denote SMS genotype and shapes indicate infection status. **(b)** Heatmap showing row-wise z-scores calculated on $\log_{10}(x + 1)$-transformed pmol/sample values across different cell lines under uninfected (-Sne) and infected (+Sne) conditions, ranging from low (blue) to high (red).

Supplementary Figure 12

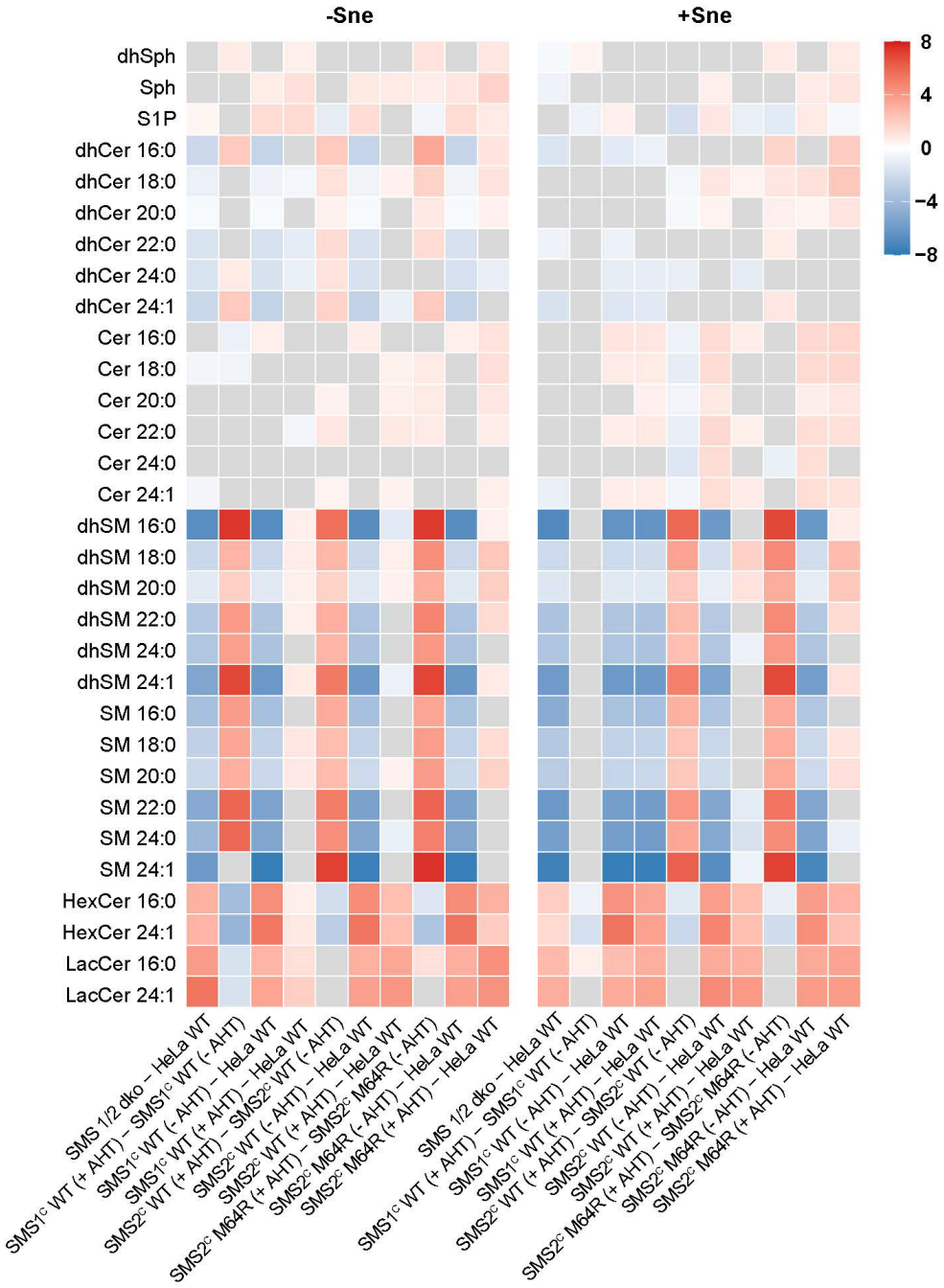

Supp. Fig. 12. Differential remodeling of individual sphingolipid species across SMS genotypes. Heatmap showing pairwise group comparisons performed on $\log_{10}(x + 1)$-transformed pmol/sample values of individual sphingolipids across SMS-modified cell lines, represented as $\log_2$ (uninfected (-Sne) and infected (+Sne)) with p-value adjusted for FDR. Pairwise comparisons were performed between SMS1/2 dko, SMS1^C WT, SMS2^C WT, and SMS2^C M64R cells relative to HeLa WT controls and under both AHT-induced (+AHT) and non-induced (-AHT) conditions. Values are displayed ranging from blue (decrease) to red (increase), with white indicating no change, and non-significant comparisons (FDR ≥ 0.05) masked (grey).

Supplementary Figure 13

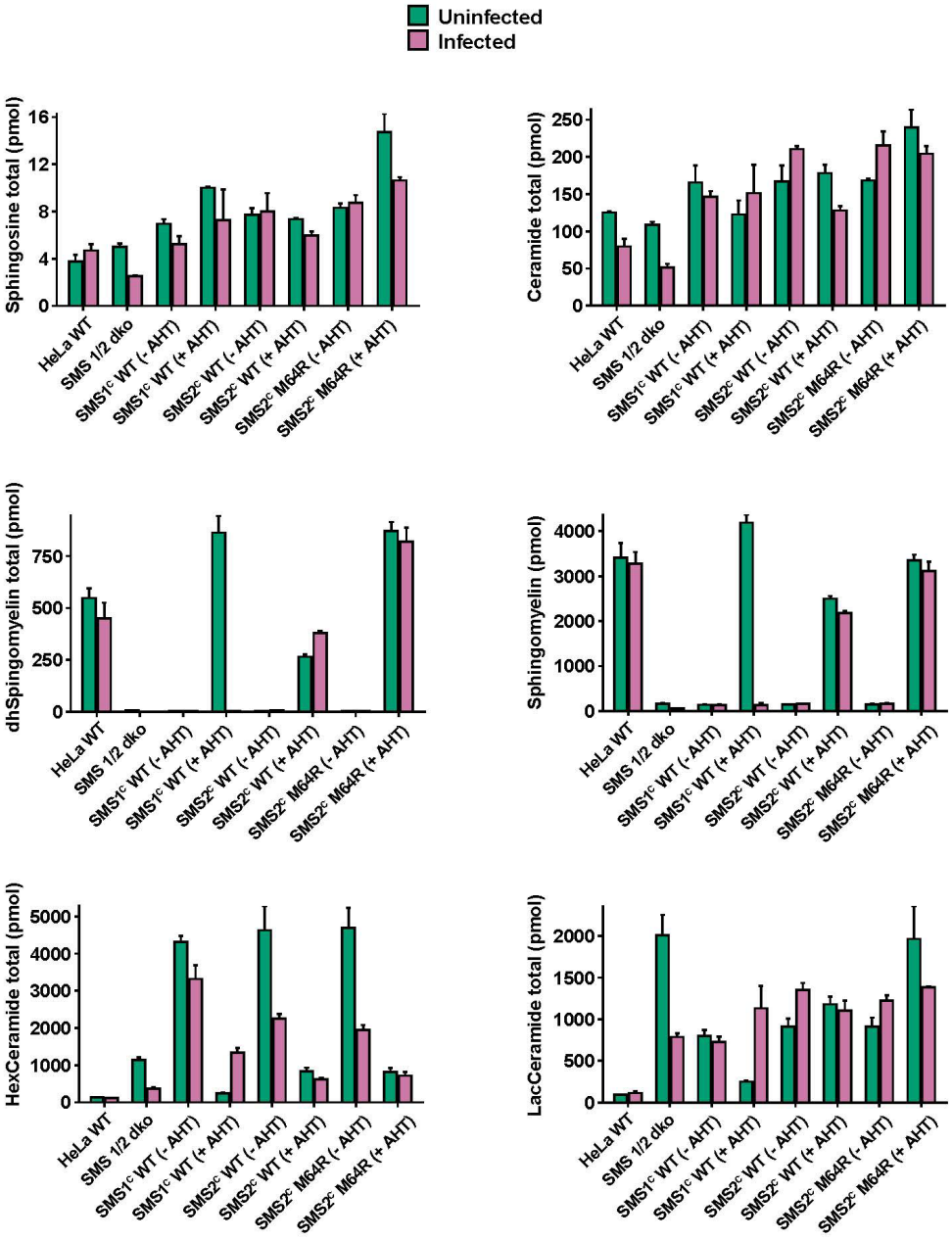

275

276 **Supp. Fig. 13. Quantitative sphingolipid class abundances across SMS genotypes during Sne infection.**
277 Quantification of sphingolipids (sphingosine, ceramide, dihydrosphingomyelin, sphingomyelin, hexosylceramide, and
278 lactosylceramide) abundances in SMS-modified HeLa cells under uninfected (green) and infected (purple) conditions.
279 Infection-dependent changes were compared across following genotypes: HeLa WT, SMS1/2 dko, SMS1^{C} WT (-
280 /+AHT), SMS2^{C} WT (-/+AHT), and SMS2^{C} M64R (-/+AHT). Lipid abundances were quantified by targeted LC-MS/MS
281 based lipidomics and expressed as pmol/sample. Bar plots represent total levels of sphingolipid classes (mean ± SD),
282 with colors indicating infection.

283

284 **Supplementary Table:1 Cell lines used**

Nr.	Cell lines	Description	Genetic modification	Method of generation	Credits/source
1.	HeLa (ATCC CCL-2™) and HeLa229 (ATCC CCL-2.1™)	Used as control for infection and lipidomics experiments	None	Standard cell culture	Lab stock
2.	HUVEC, GibcoTM, Cat. No.C01510C)	Used as a model for comparison with HeLa cells	None	Standard cell culture	Lab stock
3.	ASM KD (cl.2, cl.6)	HeLa cells with reduced acid sphingomyelinase activity	Knockdown of ASM (SMPD1)	Stable shRNA-mediated knockdown	Generated by Kerstin Paprotka and validated by Marcel Rühling.
4.	AC KO (cl.5)	HeLa cells lacking acid ceramidase activity	Knockout of AC (ASAH1)	CRISPR/Cas9-mediated gene deletion	Generated in this study.
5.	CERT KO	HeLa cells deficient in ceramide transport	Knockout of CERT (COL4A3BP)	CRISPR/Cas9-mediated gene deletion	Provided by Dagmar Heuer.
6.	SMS1/2 DKO	HeLa cells lacking SMS1&2 activity	Knockout of SMS1 (SGMS1) and SMS2 (SGMS2)	CRISPR/Cas9-mediated gene deletion	Provided by Joost Holthuis
7.	SMS1-complemented DKO	SMS1/2 DKO cells with restored SMS1 expression	Re-expression of SMS1 in DKO background	Lentiviral transduction of pInducer20-FLAG-SMS1	Generated in this study. Plasmid construct was provided by Joost Holthuis.
8.	SMS2 - complemented DKO	SMS1/2 DKO cells expressing SMS2	Re-expression of SMS2 in DKO background	Lentiviral transduction of pInducer20-FLAG-SMS2	Provided by Joost Holthuis.
9.	SMS2-M64A-complemented DKO	SMS1/2 DKO cells expressing SMS2 mutant	M64A mutation (catalytically active variant)	Lentiviral transduction	Provided by Joost Holthuis.
10.	SMS2-M64R-complemented DKO	SMS1/2 DKO cells expressing ER-mislocalized SMS2	M64R mutation (catalytically active but ER-mislocalized)	Lentiviral transduction	Provided by Joost Holthuis.
11.	U-2 OS	Used to prepare the Simkania stocks	None	Standard cell culture	Lab stock

285

286

287

Supplementary Table:2 LC-MS/MS parameters for sphingolipid quantification.

Sphingolipid	Precursor ion (*m/z*)	Product ion (*m/z*) [a]	ISTD	Calibration reference compound
d_7-Sph (ISTD)	307.3 $[M+H]^+$	289.3 / **259.3**	-	-
d_7-dhSph (ISTD)	309.4 $[M+H]^+$	291.3 / **261.3**	-	-
d_7-S1P (ISTD)	387.3 $[M+H]^+$	**271.3** / 82.1	-	-
Sph	300.3 $[M+H]^+$	282.3 / **252.3**	d_7-Sph	-
dhSph	302.3 $[M+H]^+$	284.3 / **254.3**	d_7-dhSph	-
S1P	380.3 $[M+H]^+$	**264.3** / 82.1	d_7-S1P	-
dhCer 16:0	540.5 $[M+H]^+$	522.6 / **284.3**	Cer 17:0	dhCer 16:0
dhCer 18:0	568.5 $[M+H]^+$	550.5 / **284.3**	Cer 17:0	dhCer 18:0
dhCer 20:0	596.6 $[M+H]^+$	578.6 / **284.3**	Cer 17:0	dhCer 18:0
dhCer 22:0	624.6 $[M+H]^+$	606.6 / **284.3**	Cer 17:0	dhCer 24:0
dhCer 24:0	652.7 $[M+H]^+$	634.6 / **284.3**	Cer 17:0	dhCer 24:0
dhCer 24:1	650.7 $[M+H]^+$	632.7 / **284.3**	Cer 17:0	dhCer 24:1
Cer 17:0 (ISTD)	534.5 $[M-H_2O+H]^+$	282.3 / **264.3**	-	-
Cer 16:0	520.5 $[M-H_2O+H]^+$	282.3 / **264.3**	Cer 17:0	Cer 16:0
Cer 18:0	548.5 $[M-H_2O+H]^+$	282.3 / **264.2**	Cer 17:0	Cer 18:0
Cer 20:0	576.6 $[M-H_2O+H]^+$	282.3 / **264.3**	Cer 17:0	Cer 20:0
Cer 22:0	604.6 $[M-H_2O+H]^+$	282.3 / **264.3**	Cer 17:0	Cer 22:0
Cer 24:0	632.6 $[M-H_2O+H]^+$	282.3 / **264.3**	Cer 17:0	Cer 24:0
Cer 24:1	630.6 $[M-H_2O+H]^+$	282.3 / **264.3**	Cer 17:0	Cer 24:1
dhSM 16:0	705.6 $[M+H]^+$	**184.0** / 86.1	d_{31}-SM 16:0	SM 16:0
dhSM 18:0	733.6 $[M+H]^+$	**184.0** / 86.1	d_{31}-SM 16:0	SM 18:0
dhSM 20:0	761.6 $[M+H]^+$	**184.0** / 86.1	d_{31}-SM 16:0	SM 20:0
dhSM 22:0	789.7 $[M+H]^+$	**184.0** / 86.1	d_{31}-SM 16:0	SM 22:0
dhSM 24:0	817.7 $[M+H]^+$	**184.0** / 86.1	d_{31}-SM 16:0	SM 24:0
dhSM 24:1	815.7 $[M+H]^+$	184.0 / **86.1**	d_{31}-SM 16:0	SM 24:1
d_{31}-SM 16:0 (ISTD)	734.6 $[M+H]^+$	**184.0** / 86.1	-	-
SM 16:0	703.6 $[M+H]^+$	**184.0** / 86.1	d_{31}-SM 16:0	SM 16:0
SM 18:0	731.6 $[M+H]^+$	**184.0** / 86.1	d_{31}-SM 16:0	SM 18:0
SM 20:0	759.6 $[M+H]^+$	**184.0** / 86.1	d_{31}-SM 16:0	SM 20:0
SM 22:0	787.7 $[M+H]^+$	**184.0** / 86.1	d_{31}-SM 16:0	SM 22:0
SM 24:0	815.7 $[M+H]^+$	**184.0** / 86.1	d_{31}-SM 16:0	SM 24:0
SM 24:1	813.7 $[M+H]^+$	184.0 / **86.1**	d_{31}-SM 16:0	SM 24:1
HexCer 17:0 (ISTD)	714.6 $[M+H]^+$	696.6 / **264.2**	-	-
HexCer 16:0	700.6 $[M+H]^+$	682.6 / **264.2**	HexCer 17:0	HexCer 16:0
HexCer 18:0	728.6 $[M+H]^+$	710.6 / **264.2**	HexCer 17:0	HexCer 16:0
HexCer 20:0	756.6 $[M+H]^+$	738.6 / **264.2**	HexCer 17:0	HexCer 16:0
HexCer 22:0	784.6 $[M+H]^+$	766.6 / **264.2**	HexCer 17:0	HexCer 24:1
HexCer 24:0	812.7 $[M+H]^+$	794.7 / **264.2**	HexCer 17:0	HexCer 24:1
HexCer 24:1	810.7 $[M+H]^+$	792.7 / **264.2**	HexCer 17:0	HexCer 24:1
LacCer 17:0 (ISTD)	876.6 $[M+H]^+$	534.5 / **264.3**	-	-
LacCer 16:0	862.6 $[M+H]^+$	520.5 / **264.3**	LacCer 17:0	LacCer 16:0
LacCer 18:0	890.6 $[M+H]^+$	548.5 / **264.3**	LacCer 17:0	LacCer 16:0
LacCer 20:0	918.6 $[M+H]^+$	576.6 / **264.3**	LacCer 17:0	LacCer 16:0
LacCer 22:0	946.6 $[M+H]^+$	604.6 / **264.3**	LacCer 17:0	LacCer 24:1
LacCer 24:0	974.7 $[M+H]^+$	632.6 / **264.3**	LacCer 17:0	LacCer 24:1
LacCer 24:1	972.7 $[M+H]^+$	630.7 / **264.3**	LacCer 17:0	LacCer 24:1

[a]Quantifiers are given in bold.

Cer, ceramide; dhCer, dihydroceramide; dhSM, dihydrosphingomyelin; dhSph, dihydrosphingosine; HexCer, hexosylceramide;

ISTD, internal standard; LacCer, lactosylceramide; S1P, sphingosine 1-phosphate; SM, sphingomyelin; Sph, sphingosine.

Supplementary References

1. Idkowiak, J., et al., *Best practices and tools in R and Python for statistical processing and visualization of lipidomics and metabolomics data.* Nat Commun, 2025. **16**(1): p. 8714.
2. Wei, R., et al., *GSimp: A Gibbs sampler based left-censored missing value imputation approach for metabolomics studies.* PLOS Computational Biology, 2018. **14**(1): p. e1005973.
3. van den Berg, R.A., et al., *Centering, scaling, and transformations: improving the biological information content of metabolomics data.* BMC Genomics, 2006. **7**(1): p. 142.
4. Do, K.T., et al., *Characterization of missing values in untargeted MS-based metabolomics data and evaluation of missing data handling strategies.* Metabolomics, 2018. **14**(10): p. 128.
5. Wei, R., et al., *Missing Value Imputation Approach for Mass Spectrometry-based Metabolomics Data.* Scientific Reports, 2018. **8**(1): p. 663.